

---

# Avocado: Generative Adversarial Network for Artifact-free Vocoder

---

**Taejun Bak\***

AI Center, NCSOFT

happyjun@ncsoft.com

**Junmo Lee\***

AI Center, NCSOFT

ljun4121@ncsoft.com

**Hanbin Bae**

AI Center, NCSOFT

bhb0722@ncsoft.com

**Jinhyeok Yang†**

Supertone Inc.

yangyangii@yangyangii.world

**Jae-Sung Bae†**

Samsung Research

jsbae@gmail.com

**Young-Sun Joo**

AI Center, NCSOFT

ysjoo555@ncsoft.com

## Abstract

Neural vocoders based on the generative adversarial neural network (GAN) have been widely used due to their fast inference speed and lightweight networks while generating high-quality speech waveforms. Since the perceptually important speech components are primarily concentrated in the low-frequency band, most of the GAN-based neural vocoders perform multi-scale analysis that evaluates down-sampled speech waveforms. This multi-scale analysis helps the generator improve speech intelligibility. However, in preliminary experiments, we observed that the multi-scale analysis which focuses on the low-frequency band causes unintended artifacts, e.g., aliasing and imaging artifacts, and these artifacts degrade the synthesized speech waveform quality. Therefore, in this paper, we investigate the relationship between these artifacts and GAN-based neural vocoders and propose a GAN-based neural vocoder, called Avocado, that allows the synthesis of high-fidelity speech with reduced artifacts. We introduce two kinds of discriminators to evaluate waveforms in various perspectives: a collaborative multi-band discriminator and a sub-band discriminator. We also utilize a pseudo quadrature mirror filter bank to obtain downsampled multi-band waveforms while avoiding aliasing. The experimental results show that Avocado outperforms conventional GAN-based neural vocoders in both speech and singing voice synthesis tasks and can synthesize artifact-free speech. Especially, Avocado is even capable to reproduce high-quality waveforms of unseen speakers.

## 1 Introduction

Speech synthesis also known as text-to-speech (TTS) generates speech waveforms that correspond to the input text. At first, a TTS model generates acoustic features such as a mel-spectrogram corresponding to the input text [1–3]. A vocoder then converts the acoustic features into a speech waveform [4–8]. With the introduction of deep learning, neural vocoders can now generate high-fidelity speech waveforms that are indistinguishable from human recordings [7–9].

Recently, GAN-based vocoders with non-autoregressive convolutional architectures have been proposed [10–16]. Comparing the previous neural vocoders [6–9], these models are faster, lighter, and can generate high-quality waveforms. Specifically, the generator converts input features such as random noise or a mel-spectrogram into speech waveforms. The discriminator then evaluates the

---

\*Equal contribution.

†Work performed at NCSOFT.

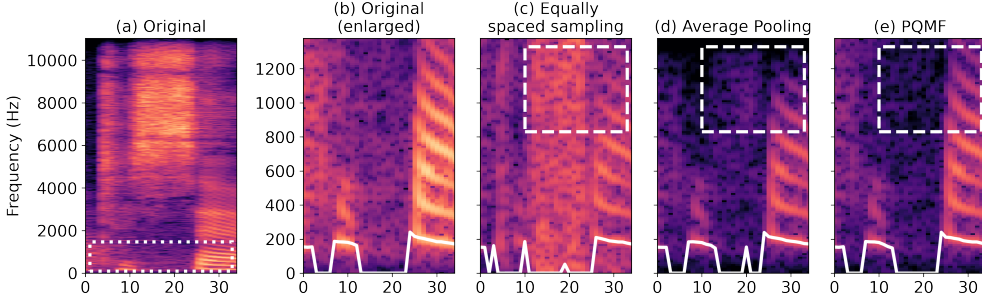


Figure 1: The spectrograms of original and downsampled audio samples. White solid lines are contours of  $F_0$ . We perform downsampling of (a) the original waveform with (c) the equally spaced sampling, (d) the average pooling, and (e) PQMF.

generated speech waveforms. In MelGAN [11], focusing on multi-scale analysis, a multi-scale discriminator (MSD) evaluates the downsampled waveforms using an average pooling technique. In HiFi-GAN [12], a multi-period discriminator (MPD) specializing in periodic components was proposed. It discriminates downsampled waveforms using an equally spaced sampling technique with various periods.

Downsampling limits the frequency range of speech by decreasing the sampling rate [17]. Because the speech spectrum in the low-frequency bands has a much more important impact on perceptual quality, GAN-based vocoders perform multi-scale analysis that evaluates the downsampled waveforms along with the full-band waveform. The multi-scale analysis allows the generator to focus on the speech spectrum in the low-frequency bands. Consequently, these GAN-based vocoders have been successful in increasing the quality of synthesized speech [11–13, 16, 18].

However, GAN-based vocoders suffer from two major problems. The first is that of the degraded reproducibility of the harmonic components. The fundamental frequency ( $F_0$ ) of synthesized speech is often inaccurate [19], aliasing occurring during downsampling being one of the reasons for this problem. The second problem is that of a lack of reproducibility at high-frequency bands. For example, imaging artifacts at high-frequency bands can degrade the speech quality with noisy sound. The training objective which rely on the low-frequency band obtained by simple downsampling techniques aggravates these two problems. In Section 2, we further analyzed the aforementioned problems.

To address these issues, we propose a neural vocoder called Avocado, which specializes in learning various frequency features. By minimizing artifacts, Avocado synthesizes speech with the improved quality. We propose two discriminators; a collaborative multi-band discriminator (CoMBD) and a sub-band discriminator (SBD). The CoMBD performs multi-scale analysis in a balanced manner and suppress artifacts with a novel structure. The SBD contributes to improve the sound quality by discriminating frequency-wise decomposed waveforms. Additionally, we utilize a pseudo quadrature mirror filter bank (PQMF) equipped with high stopband attenuation suppressing aliasing to obtain downsampled and decomposed waveforms in the training process. Owing to the proposed discriminators and the utilization of the PQMF, the generator learns exactly the speech spectrum not only in the low-frequency bands but also in the high-frequency bands. Therefore, Avocado can synthesize artifact-free speech in speech and singing voice synthesis tasks, while being robust in unseen speaker synthesis.

## 2 Artifacts in GAN-based Vocoder

### 2.1 Aliasing in downsampling

GAN-based vocoders use discriminators to evaluate downsampled waveforms to learn the spectral information in low-frequency bands. Typical downsampling methods include the average pooling used in [11–13] or the equally spaced sampling used in [12, 16, 18]. They are easy to implement and efficient for obtaining band-limited speech waveforms. However, in our preliminary experiments, aliasing was observed in the downsampled waveforms using the above methods.

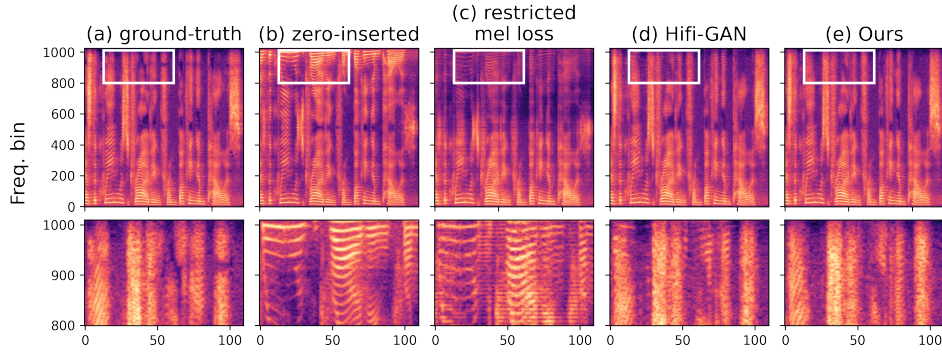


Figure 2: Sub-figures in the first row show spectrograms of (a) a ground truth, generated waveforms from (b) a zero-stuffing, (c) model trained with restricted mel-reconstruction loss, (d) HiFi-GAN, and (e) proposed methods. The enlarged version of the white rectangular box is depicted in the second row, mirrored low-frequencies in (b) still exist in results from (c) and (d), but not from (e).

Figure 1 shows examples of the downsampled waveforms using several approaches; the downampling factor is set to 8. When downampling using equally spaced sampling (Figure 1c), high-frequency components that are supposed to be removed, fold back and distort the harmonic frequency components at a low-frequency band. In the case of the average pooling (Figure 1d), which is a composition of a simple low-pass filtering and a decimation, aliasing is not that noticeable at a low-frequency band but harmonic components over 800Hz are distorted. As the downampling factor increases, the artifacts increase too. Using these distorted waveforms during the training makes it difficult for the model to generate accurate waveforms.

To avoid aliasing, downampling using a band-pass filter equipped with high stopband attenuation is required. The PQMF [20] is a digital filter that satisfies this requirement [14, 21]. Downsampling using the PQMF well preserves the harmonics, as shown in Figure 1d.

## 2.2 Imaging artifact in upsampling

GAN-based vocoders include upsampling layers in their structure to increase the rate of input features, such as a mel-spectrogram, up to the sampling rate of the waveform [11–16]. During the upsampling process, low-frequency components are mirrored to the high-frequency bands after an expansion by zero-insertion, as shown in Figure 2b. Then, in the filtering stage, these frequency components should be removed. In GAN-based vocoders, upsampling layers such as a transposed convolution take these processes. However, because the upsampling layers are insufficient to remove them, unintended frequency components remain. In this paper, we call these remained frequency components at the high-frequency bands as *imaging artifacts*. Such artifacts are similar to texture sticking of image generative models, which was reported in [22]. The imaging artifacts also degrade the speech quality, causing distortions in the high-frequency band.

The GAN-based vocoders also suffer from these artifacts as shown in Figure 2d. We hypothesized that the training objective with discriminators relying on low-frequency features accentuates these artifacts, making the generator concentrate on modeling low-frequencies more so than the filtering. We found that the similar artifact occurred as shown in Figure 2c, when the generator trained with the mel reconstruction loss limited to the lower half of the frequency band excluding the discriminator-related losses. Therefore, we attempt to suppress the artifacts by training the generator in a balanced manner.

## 3 Proposed Method

Figure 3 describes the overall architecture of Avocodo. It has a single generator and the proposed two discriminators. Taking a mel-spectrogram as input, the generator outputs not only a full-resolution waveform but also intermediate outputs. Then the CoMBD discriminates the full-resolution waveform and its downsampled waveforms along with the intermediate outputs. The PQMF is used as a low-pass

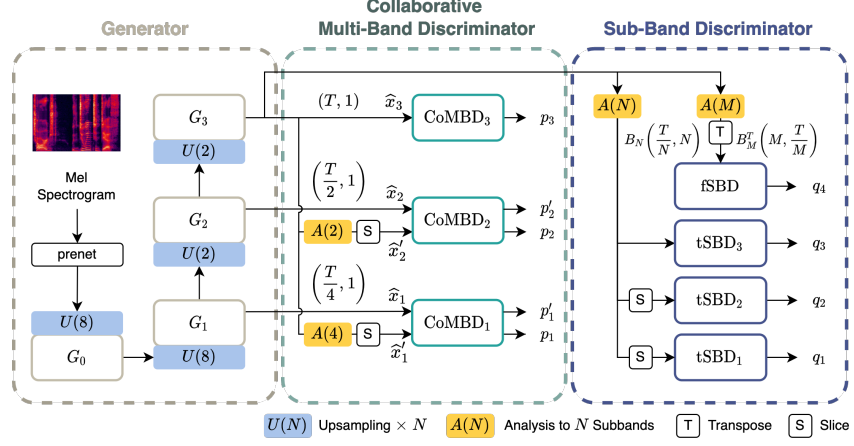


Figure 3: Overall Architecture of Avocado.

filter to downsample the full-resolution waveform. Additionally, the SBD discriminates sub-band signals obtained by the PQMF analysis.

### 3.1 Generator

The proposed generator follows the structure of the HiFi-GAN generator, but it produces multi-scale outputs that are a full-resolution waveform and intermediate outputs. The generator has four sub-blocks, three of which  $G_k (1 \leq k \leq 3)$  generate waveforms  $\hat{x}_k$  with the corresponding resolution of  $\frac{1}{2^{3-k}}$  of the full-resolution; that is  $\hat{x}_3$  is a full-resolution waveform, and  $\hat{x}_1$  and  $\hat{x}_2$  denote intermediate outputs. Each sub-block is composed of multi-receptive field fusion (MRF) blocks [12] and transposed convolution layers. The MRF blocks consist of multiple residual blocks of diverse kernel sizes and dilation rates to capture the spatial features of the input. Note that we add additional projection layers, unlike HiFi-GAN, after each sub-block to return the intermediate outputs.

### 3.2 Collaborative Multi-Band Discriminator

The proposed CoMBD discriminates multi-scale outputs from the generator. It comprises identical sub-modules which evaluate waveforms at different resolutions. Each sub-module consists of fully convolutional layers and a leaky ReLU activation function. Further details are provided in Appendix A.1.

A multi-scale structure (Figure 4a) or a hierarchical structure (Figure 4b) are commonly used in conventional GAN-based neural vocoders, respectively, but in this paper, we combine the two structures taking advantage of each structure as shown in Figure 4c. This collaborative structure of multi-scale and hierarchical arrangements helps the generator synthesize high-quality waveforms with reduced artifacts.

The multi-scale structure increases speech quality by discriminating not only the full-resolution waveform but also the downsampled waveform [11, 12, 14, 18]. Specifically, discriminating the waveforms downsampled into multiple scales helps the generator focus on the spectral features in low-frequency band [11]. Meanwhile, the hierarchical structure uses intermediate output waveforms of each generator sub-block. It helps the generator learn the various levels of acoustic properties in a balanced manner [13, 23]. Specifically, the generator sub-blocks are trained to learn expansion and filtering in a balanced way by inducing the sub-blocks of the generator to generate a band-limited waveform. Therefore, it is expected to suppressing the imaging artifacts in Section 2.2 by adopting the hierarchical structure.

For the collaborative structure, the sub-modules at low resolution, i.e., CoMBD<sub>1</sub> and CoMBD<sub>2</sub>, take both the intermediate outputs  $\hat{x}$  and the downsampled waveforms  $\hat{x}'$  as their inputs. For each resolution, both inputs share the sub-module. For example, as shown in Figure 3 intermediate outputs  $\hat{x}_2$  and downsampled waveform  $\hat{x}'_2$  share weights of CoMBD<sub>2</sub> for output  $p_2$  and  $p'_2$ . As in [24], we intend that, by the collaboration, the intermediate output waveforms and downsampled waveforms

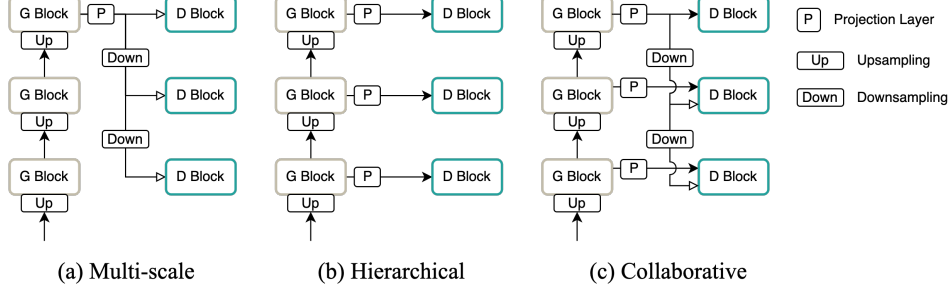


Figure 4: Comparison on various structure of discriminators.

become the same as each other. Note that no additional parameters are necessary for the collaboration of the two structures because of the weight-sharing process.

To further improve speech quality by reducing artifacts, we adopt a differentiable PQMF to obtain downsampled waveform with restricted aliasing. First, we decompose a full-resolution speech waveform into  $N$  sub-band signals  $B_N$  by using the PQMF analysis. The  $B_N$  consists of single-band signals  $b_1, \dots, b_N$  whose length is  $\frac{T}{N}$ , where  $T$  is the length of the full-resolution waveform [20]. Then, we select the first sub-band signal  $b_1$  corresponding to the lowest frequency band.

### 3.3 Sub-Band Discriminator

We introduce a SBD that discriminates multiple sub-band signals by PQMF analysis. The PQMF enables the  $n^{th}$  sub-band signal  $b_n$  to contain frequency information corresponding to the range from  $(n-1)f_s/2N$  to  $nf_s/2N$ , where  $f_s$  is the sampling frequency and  $N$  is the number of sub-bands. Inspired by this characteristic of sub-band signals, sub-modules of the SBD learn various discriminative features by using different ranges of the sub-band signals.

We design two types of sub-modules: one captures the spectral feature's changes over the time axis and the other captures the relationship between each sub-band signal. These two sub-modules are referred to as tSBD and fSBD, respectively, in Figure 3. The tSBD takes  $B_N$  as its input and performs time-domain convolution with  $B_N$ . By diversifying the sub-band ranges, we can design each sub-module to learn the characteristics of the specific frequency range. In other words,  $tSBD_k$  takes the certain number of sub-band signals  $b_{i_k:j_k}$  as its input. By contrast, fSBD takes the transposed version of  $M$  channel sub-bands  $B_M^T$ . The composition of fSBD is inspired by the spectral features of the speech waveform, such as harmonics and formants.

Each sub-module of the SBD is composed of stacked multi-scale dilated convolution banks [25] to evaluate the sub-band signals. The dilated convolution bank contains convolution layers with different dilation rates that cover diverse receptive fields. The architecture of the SBD follows an inductive bias in that accurate analysis on speech waveforms requires various receptive fields for each frequency range. Consequently, we use different dilation factors prepared for each sub-module. Further details are provided in Appendix A.2.

Several neural vocoders utilize filter-banks to decompose speech waveforms and discriminators to inspect the sub-band signals [14–16]. In particular, the SBD is similar to the filter-bank random window discriminators (FB-RWDs) of the StyleMeGAN [15] in that both obtain sub-band signals using the PQMF. However, there is a considerable difference between the SBD and FB-RWDs. Each sub-module of the SBD evaluates a different range of sub-band signals, whereas the FB-RWDs varies the number of sub-band signals for each discriminator. In addition, the SBD has many types of blocks: blocks used to observe a lower frequency band, a whole range of frequency bands, and a relationship between frequency bands. Consequently, the SBD can evaluate the signals more effectively.

### 3.4 Training Objectives

**GAN Loss** For training GAN networks, we use the LSGAN [26] that replaces a sigmoid cross-entropy term of the GAN training objective proposed in [27] with the least square for stable GAN training. The GAN losses  $V$  for multi-scale outputs and  $W$  for downsampled waveform are defined

as follows:

$$\begin{aligned} V(D_k; G) &= \mathbb{E}_{(x_k, s)} \left[ (D_k(x_k) - 1)^2 + (D_k(\hat{x}_k))^2 \right], \quad V(G; D_k) = \mathbb{E}_s \left[ (D_k(\hat{x}_k) - 1)^2 \right], \\ W(D_k; G) &= \mathbb{E}_{(x_k, s)} \left[ (D_k(x_k) - 1)^2 + (D_k(\hat{x}'_k))^2 \right], \quad W(G; D_k) = \mathbb{E}_s \left[ (D_k(\hat{x}'_k) - 1)^2 \right] \end{aligned} \quad (1)$$

where  $x_k$  represents the  $k^{th}$  downsampled ground-truth waveform, and  $s$  denotes the speech representation. In this paper we used a mel-spectrogram.

**Feature Matching Loss** Feature matching loss is a perceptual loss for GAN training [28]. This perceptual loss has been used in GAN-based vocoder systems [11–13]. Finally, the feature matching loss of a sub-module in the discriminator can be established with L1 differences between the intermediate feature maps of the ground-truth and predicted. The loss can be defined as follows:

$$L_{fm}(G; D_t) = \mathbb{E}_{(x, s)} \left[ \sum_{t=1}^T \frac{1}{N_t} \|D_t(x) - D_t(\hat{x})\|_1 \right], \quad (2)$$

where  $T$  denotes the number of layers in a sub-module.  $D_t$  and  $N_t$  represents the  $t^{th}$  feature map and the number of elements in the feature map, respectively.

**Reconstruction Loss** Reconstruction loss based on a mel-spectrogram increases the stability and efficiency in the training of waveform generation [10]. We calculate the L1 differences between the mel-spectrogram of the ground-truth speech waveform  $x$  and the mel-spectrogram of the predicted speech waveform  $\hat{x}$ . When  $\phi(\cdot)$  represents a function of the transform to the mel-spectrogram, the reconstruction loss can be expressed as follows:

$$L_{spec}(G) = \mathbb{E}_{(x, s)} \left[ \|\phi(x) - \phi(\hat{x})\|_1 \right]. \quad (3)$$

**Final Loss** Final loss for the overall system training can be established from the aforementioned loss terms and defined as follows:

$$\begin{aligned} L_D^{total} &= \sum_{p=1}^P V(D_p^C; G) + \sum_{p=1}^{P-1} W(D_p^C; G) + \sum_{q=1}^Q V(D_q^S; G), \\ L_G^{total} &= \sum_{p=1}^P \left[ V(G; D_p^C) + \lambda_{fm} L_{fm}(G; D_p^C) \right] + \sum_{p=1}^{P-1} \left[ W(G; D_p^C) + \lambda_{fm} L_{fm}(G; D_p^C) \right] \\ &\quad + \sum_{q=1}^Q \left[ V(G; D_q^S) + \lambda_{fm} L_{fm}(G; D_q^S) \right] + \lambda_{spec} L_{spec}(G), \end{aligned} \quad (4)$$

where  $D_p^C$  and  $D_q^S$  denote  $p^{th}$  sub-module of CoMBD and  $q^{th}$  sub-module of SBD, respectively.  $\lambda_{fm}$  and  $\lambda_{spec}$  denote the loss scales for the feature matching loss and reconstruction loss, respectively. We set  $\lambda_{fm}$  to 2, and  $\lambda_{spec}$  to 45.

## 4 Experiments

### 4.1 Datasets

**Single speaker speech synthesis** The LJSpeech [29] dataset was used for a single speaker experiment. The dataset was recorded by native English-speaking female speaker with total amount of 24 hours. It contains 13,100 audio samples and 150 samples were taken for the test dataset.

**Singing voice synthesis** An internal singing dataset was used to verify the ability to synthesize large variations in vocal attributes such as pitch, duration, and amplitude. It contains of about 8500 samples recorded by 16 speakers.

**Unseen speaker speech synthesis** An internal multi-speaker Korean dataset was used to evaluate the generalization of the model. The dataset contains 156 gender-balanced speakers with amount of about 244 hours long. Among them 16 unseen speakers were excluded from training. The voice style of dataset consists of a variety of reading, daily conversations, and acting. Audio samples in overall datasets were sampled at 22,050Hz, 16bit PCM.

Table 1: The results of subjective evaluations with 95% CI, the number of parameters and inference speed on CPU and GPU.

Model	MOS (CI)		# G Param (M)	# D Param (M)	Inference Speed (CPU)	Inference Speed (GPU)
	LJ	Unseen				
Ground Truth	4.373±0.06	4.562±0.05	-	-	-	-
VocGAN	4.162±0.06	4.049±0.07	7.06	12.03	3.26x	235.0x
HiFi-GAN V1	4.270±0.06	3.709±0.07	13.94	70.72	2.98x	157.6x
HiFi-GAN V2	4.010±0.06	3.516±0.07	0.93	-	10.56x	541.2x
Avocodo V1	<b>4.285±0.06</b>	<b>4.051±0.06</b>	13.94	27.07	2.93x	156.3x
Avocodo V2	4.087±0.06	3.558±0.07	0.93	-	10.09x	539.6x

## 4.2 Training Setup

Avocodo and baseline models were trained to synthesize waveforms from ground-truth mel-spectrograms. GAN-based vocoders, HiFi-GAN and VocGAN, were selected as the baseline models. We calculated 80 bands of mel-spectrograms from audio samples with the short-time Fourier transform (STFT). The STFT parameters were set to 1024, 1024, and 256 for FFT, window, and hop size, respectively. Each audio samples were sliced with a random window selection method. The segment size was 8192 which is about 0.4 seconds long. For the singing dataset, the segment size increased to 65,536 which is about 3 seconds, because singing voices have a long vowel duration [30].

All models were trained up to 3M steps with the official implementation. We used an AdamW optimizer [31] with an initial learning rate of 0.002. The optimizer parameter  $(\beta_1, \beta_2)$  were set to  $(0.8, 0.99)$ , and the exponential learning rate decay was applied using 0.999 [12]. The hyper-parameter of the generator was the same as that of the HiFi-GAN. The HiFi-GAN generator has two versions having an identical architecture but differing number of parameters: V1 is larger than V2 and Avocodo also follows this rule. The number of sub-band  $N$  is 16 for tSBD and is  $M = 64$  for fSBD. The parameters of the PQMF were empirically selected. Detailed explanations are provided in Appendix B.

## 5 Results

### 5.1 Audio Quality & Comparison

The performance of the mel-spectrogram for waveform inversion for each dataset was assessed using subjective and objective measurements<sup>3</sup>. 5-scale mean opinion score (MOS) test was conducted for the single and unseen speakers speech synthesis and a comparative MOS (CMOS) test was conducted for the singing voice synthesis. For CMOS, participants were requested to rate scores varying from  $-3$  (meaning that the sample from HiFi-GAN is more similar to ground-truth) to  $+3$  (meaning opposite). For the English dataset, 19 native English speakers participated via Amazon Mechanical Turk and for the Korean datasets 19 native Korean speakers participated. Objective evaluations were conducted to quantitatively compare vocoders. To validate the reproducibility of the fundamental frequencies ( $F_0$ ), we measured the root mean square error of  $F_0$  ( $F_0$  RMSE), false positive and negative rate of the voice/unvoice classification ( $VUV_{fpr}$ ,  $VUV_{fnr}$ ). To measure the perceived quality of the synthesized speech, the mel-cepstral distortion (MCD)[32], structural similarity index (SSIM)[33], perceptual evaluation of speech quality (PESQ)[34] and short-time objective intelligibility (STOI)[35] were calculated.

**Single speaker speech synthesis** Both subjective and objective evaluation results in single speaker speech synthesis compared to the baselines are presented in Table 1 and Table 2, respectively. AvocodoV1 outperformed HiFi-GAN and VocGAN in MOS tests. It reduced the imaging artifact considerably, as shown in Figure 2e, compared to the HiFi-GAN as shown in Figure 2d. AvocodoV2 also outperformed HiFi-GANV2.

<sup>3</sup> Audio samples are available at <https://nc-ai.github.io/speech/publications/Avocodo/index.html>.

Table 2: Results of objective evaluations

Single speaker speech synthesis							
Model	$F_0$ RMSE( $\downarrow$ )	MCD( $\downarrow$ )	VUV <sub>fpr</sub> ( $\downarrow$ )	VUV <sub>fnr</sub> ( $\downarrow$ )	SSIM( $\uparrow$ )	PESQ( $\uparrow$ )	STOI( $\uparrow$ )
VocGAN	37.51	2.63	20.154	12.445	0.882	3.25	0.9614
HiFi-GAN V1	35.96	2.25	18.670	11.133	0.939	3.64	0.9819
HiFi-GAN V2	37.26	2.86	20.618	12.174	0.878	2.98	0.9648
Avocodo V1	<b>33.98</b>	<b>2.06</b>	<b>17.741</b>	<b>10.115</b>	<b>0.953</b>	<b>3.81</b>	<b>0.9866</b>
Avocodo V2	37.63	2.59	20.691	11.478	0.899	3.11	0.9709

Singing voice synthesis							
Model	$F_0$ RMSE( $\downarrow$ )	MCD( $\downarrow$ )	VUV <sub>fpr</sub> ( $\downarrow$ )	VUV <sub>fnr</sub> ( $\downarrow$ )	SSIM( $\uparrow$ )	PESQ( $\uparrow$ )	STOI( $\uparrow$ )
HiFi-GAN V1	27.86	2.67	12.075	2.044	0.9155	3.48	<b>0.8125</b>
Avocodo V1	<b>26.88</b>	<b>2.42</b>	<b>10.57</b>	<b>1.74</b>	<b>0.931</b>	<b>3.55</b>	0.8052

Table 3: CMOS results of singing voice synthesis with 95% CI.

(-)	CMOS (CI)	(+)
HiFi-GAN V1	0.403 ( $\pm 0.06$ )	Avocodo V1

Table 4: MOS results of ablation study with 95% CI.

Model	MOS (CI)
MSD[11]	3.743 ( $\pm 0.07$ )
MPD[12]	3.675 ( $\pm 0.08$ )
CoMBD	4.156 ( $\pm 0.05$ )
SBD	4.130 ( $\pm 0.06$ )

In the objective evaluation, AvocodoV1 also outperformed HiFi-GAN and VocGAN. Avocodo improved the overall results in both versions. Especially, It decreased MCD by approximately 9%.

Despite the small number of parameters in discriminators, Avocodo shows better performance than HiFi-GAN in every version. Note that the parameter number of generator slightly increased for projection layer at intermediate layers. We measured inference time in CPU (Intel i7 CPU 3.00GHz) and a single GPU (NVIDIA V100) environments. There was not much difference in inference time between Avocodo and HiFi-GAN.

**Singing voice synthesis** Table 3 and Table 2 show that Avocodo synthesized singing voice that more reflects the target singing style than the baseline. Avocodo was successful in generating the artifact-free high frequency components and clear pitch contour. Additionally, we observed the performance difference in reconstructing higher-pitch voice and provide further analysis in Appendix C.

**Unseen speaker synthesis** To verify generalization to unseen data, we conducted MOS tests in unseen speaker synthesis. In Table 1, the MOS results show that AvocodoV1 outperformed HiFi-GAN and VocGAN. VocGAN also shows similar performance in generalization. However, AvocodoV1 shows the best performance in both single and unseen speaker synthesis tasks. The results of HiFi-GAN fall behind other vocoders due to its inconsiderable downsampling methods and multi-scale analysis. Therefore, we confirmed that the proposed vocoder is more robust in the unseen dataset.

## 5.2 Ablation Study

To observe the performance changes based on the composition of the proposed discriminator and PQMF, every discriminator was trained using the generator of Avocodo V2. We observed empirically that  $\lambda_{fm}$  and  $\lambda_{spec}$  also affects the training, so they were adjusted to 2 and 10, respectively. However,  $\lambda_{spec}$  was adjusted to 20 for the CoMBD which has a larger loss value owing to weight-sharing.

First, we compared the effect of downsampling methods and the structure of the discriminators. The results in Table 5 show that the harmonic components were well reproduced when the PQMF was used than Average Pooling (AP) was used. The multi-scale structure was more helpful for improving the perceptual quality than the hierarchical structure. However, we observed that the imaging artifact was reduced in the hierarchical structure, especially, when the PQMF was used together. Having the hierarchical structure and PQMF, the CoMBD gets better scores in every measurement. Therefore, we confirmed that CoMBD contributes to not only increasing the quality but also restricting artifacts.

Table 5: Results of objective evaluations for ablation study. Every models were trained with the generator of  $V2$ .

Model	$F_0$ RMSE( $\downarrow$ )	MCD( $\downarrow$ )	VUV <sub>fpr</sub> ( $\downarrow$ )	VUV <sub>fnr</sub> ( $\downarrow$ )	SSIM( $\uparrow$ )	PESQ( $\uparrow$ )	STOI( $\uparrow$ )	
MSD[11]	36.45	3.91	21.29	12.33	0.830	2.58	0.951	
MPD[12]	37.02	3.91	22.15	12.07	0.840	2.62	0.953	
AP	Multi-scale	39.26	2.93	22.65	12.06	0.867	2.72	0.961
	Hierarchical	39.65	3.12	22.29	12.10	0.842	2.60	0.956
PQMF	Multi-scale	38.30	3.02	21.78	11.70	0.855	2.70	0.959
	Hierarchical	36.92	3.10	21.30	11.91	0.847	2.62	0.957
CoMBD		37.20	2.85	21.74	11.58	0.870	2.88	0.965
tSBD		36.08	2.78	20.65	11.57	0.887	2.95	0.964
tSBD+fsBD		36.05	2.84	21.49	11.20	0.882	2.97	0.964

Second, in the comparison of the composition of SBD, fsBD improves  $F_0$  RMSE slightly, but MCD degrades. However, tSBD+fsBD helped improve the sound quality while suppressing band noise can be seen in frequency bands above 5 kHz. Finally, we compared existing discriminators and the CoMBD and SBD. The discriminator of Avocodo outperform MBD and MSD in MOS and objective evaluations, as shown in Table 4 and Table 5, respectively.

## 6 Conclusions

In this paper, we proposed an artifact-free GAN-based vocoder, Avocodo. Two artifacts which degrade the synthesized speech quality were defined as aliasing and imaging artifact. We found that the artifacts originated from the objective function biased on the low-frequency band and naive downsampling method. To solve these problems, we designed two novel discriminators: CoMBD and SBD. The CoMBD has a collaborative structure combining both multi-scale and hierarchical structures. The SBD discriminates the sub-band signals decomposed by PQMF analysis in both time and frequency aspects. These discriminators enable the generator to synthesize artifact-free waveforms. We conducted experiments on various datasets each assuming different cases, and verified the performance of Avocodo. In both subjective and objective evaluations, Avocodo outperformed the baseline vocoders both in single and unseen speaker synthesis tasks. Additionally, it could synthesize singing voices whose high harmonic components are well preserved. Although Avocodo showed improved rendition compared to the baseline vocoders, the proposed methods were limited to increasing the performance with a smaller generator. In singing speaker synthesis, discontinuities on  $F_0$  were observed. We assume that it is a limitation of a generator structure (i.e., hidden dimension and receptive field size). Therefore, finding artifact-free generator architecture will be our future work.

## References

- [1] Yuxuan Wang, R. J. Skerry-Ryan, Daisy Stanton, Yonghui Wu, Ron J. Weiss, Navdeep Jaitly, Zongheng Yang, Ying Xiao, Zifeng Chen, Samy Bengio, Quoc V. Le, Yannis Agiomyrgianakis, Rob Clark, and Rif A. Saurous. Tacotron: Towards end-to-end speech synthesis. In *Interspeech*, pages 4006–4010. ISCA, 2017.
- [2] Yi Ren, Yangjun Ruan, Xu Tan, Tao Qin, Sheng Zhao, Zhou Zhao, and Tie-Yan Liu. FastSpeech: Fast, robust and controllable text to speech. In *Advances in Neural Information Processing Systems*, volume 32, 2019.
- [3] Yi Ren, Chenxu Hu, Xu Tan, Tao Qin, Sheng Zhao, Zhou Zhao, and Tie-Yan Liu. FastSpeech 2: Fast and high-quality end-to-end text to speech. In *International Conference on Learning Representations*, 2021.
- [4] Morise Masanori, Fumiya Yokomori, and Kenji Ozawa. WORLD: a vocoder-based high-quality speech synthesis system for real-time applications. *IEICE TRANSACTIONS on Information and Systems*, 99(7):1877–1884, 2016.
- [5] Hideki Kawahara. STRAIGHT, exploitation of the other aspect of vocoder: Perceptually isomorphic decomposition of speech sounds. *Acoustical science and technology*, 27(6):349–353, 2006.
- [6] Aäron van den Oord, Sander Dieleman, Heiga Zen, Karen Simonyan, Oriol Vinyals, Alex Graves, Nal Kalchbrenner, Andrew W. Senior, and Koray Kavukcuoglu. WaveNet: A generative model for raw audio. In *ISCA Speech Synthesis Workshop*, page 125. ISCA, 2016.
- [7] Ryan Prenger, Rafael Valle, and Bryan Catanzaro. WaveGlow: A flow-based generative network for speech synthesis. In *International Conference on Acoustics, Speech and Signal Processing*, pages 3617–3621. IEEE, 2019.
- [8] Sungwon Kim, Sang-Gil Lee, Jongyoon Song, Jaehyeon Kim, and Sungroh Yoon. FloWaveNet : A generative flow for raw audio. In Kamalika Chaudhuri and Ruslan Salakhutdinov, editors, *International Conference on Machine Learning*, volume 97 of *Proceedings of Machine Learning Research*, pages 3370–3378. PMLR, 09–15 Jun 2019.
- [9] Aaron van den Oord, Yazhe Li, Igor Babuschkin, Karen Simonyan, Oriol Vinyals, Koray Kavukcuoglu, George van den Driessche, Edward Lockhart, Luis Cobo, Florian Stimberg, Norman Casagrande, Dominik Grewe, Seb Noury, Sander Dieleman, Erich Elsen, Nal Kalchbrenner, Heiga Zen, Alex Graves, Helen King, Tom Walters, Dan Belov, and Demis Hassabis. Parallel WaveNet: Fast high-fidelity speech synthesis. In *International Conference on Machine Learning*, volume 80 of *Proceedings of Machine Learning Research*, pages 3918–3926. PMLR, 10–15 Jul 2018.
- [10] Ryuichi Yamamoto, Eunwoo Song, and Jae-Min Kim. Parallel WaveGAN: A fast waveform generation model based on generative adversarial networks with multi-resolution spectrogram. In *International Conference on Acoustics, Speech and Signal Processing*, pages 6199–6203. IEEE, 2020.
- [11] Kundan Kumar, Rithesh Kumar, Thibault de Boissiere, Lucas Gestin, Wei Zhen Teoh, Jose Sotelo, Alexandre de Brébisson, Yoshua Bengio, and Aaron C Courville. MelGAN: Generative adversarial networks for conditional waveform synthesis. In H. Wallach, H. Larochelle, A. Beygelzimer, F. d’Alché-Buc, E. Fox, and R. Garnett, editors, *Advances in Neural Information Processing Systems*, volume 32. Curran Associates, Inc., 2019.
- [12] Jungil Kong, Jaehyeon Kim, and Jaekyoung Bae. HiFi-GAN: Generative Adversarial Networks for Efficient and High Fidelity Speech Synthesis. In *Advances in Neural Information Processing Systems*, volume 33, pages 17022–17033, 2020.
- [13] Jinhyeok Yang, Junmo Lee, Youngik Kim, Hoon-Young Cho, and Injung Kim. VocGAN: A High-Fidelity Real-Time Vocoder with a Hierarchically-Nested Adversarial Network. In *Interspeech*, pages 200–204, 2020.

[14] Geng Yang, Shan Yang, Kai Liu, Peng Fang, Wei Chen, and Lei Xie. Multi-band MelGAN: Faster waveform generation for high-quality text-to-speech. In *Spoken Language Technology Workshop*, pages 492–498. IEEE, 2021.

[15] Ahmed Mustafa, Nicola Pia, and Guillaume Fuchs. StyleMelGAN: An efficient high-fidelity adversarial vocoder with temporal adaptive normalization. In *International Conference on Acoustics, Speech and Signal Processing*, pages 6034–6038. IEEE, 2021.

[16] Ji-Hoon Kim, Sang-Hoon Lee, Ji-Hyun Lee, and Seong-Whan Lee. Fre-GAN: Adversarial Frequency-Consistent Audio Synthesis. In *Interspeech*, pages 2197–2201, 2021.

[17] Claude Elwood Shannon. Communication in the presence of noise. *Proceedings of the IRE*, 37(1):10–21, 1949.

[18] Won Jang, Dan Lim, Jaesam Yoon, Bongwan Kim, and Juntae Kim. UnivNet: A Neural Vocoder with Multi-Resolution Spectrogram Discriminators for High-Fidelity Waveform Generation. In *Interspeech*, pages 2207–2211, 2021.

[19] Max Morrison, Rithesh Kumar, Kundan Kumar, Prem Seetharaman, Aaron Courville, and Yoshua Bengio. Chunked autoregressive GAN for conditional waveform synthesis. In *International Conference on Learning Representations*, 2022.

[20] T.Q. Nguyen. Near-perfect-reconstruction pseudo-qmf banks. *IEEE Transactions on Signal Processing*, 42(1):65–76, 1994.

[21] Chengzhu Yu, Heng Lu, Na Hu, Meng Yu, Chao Weng, Kun Xu, Peng Liu, Deyi Tuo, Shiyin Kang, Guangzhi Lei, et al. DurIAN: Duration informed attention network for multimodal synthesis. *arXiv preprint arXiv:1909.01700*, 2019.

[22] Tero Karras, Miika Aittala, Samuli Laine, Erik Härkönen, Janne Hellsten, Jaakko Lehtinen, and Timo Aila. Alias-free generative adversarial networks. In *Advances in Neural Information Processing Systems*, volume 34, 2021.

[23] Zizhao Zhang, Yuanpu Xie, and Lin Yang. Photographic text-to-image synthesis with a hierarchically-nested adversarial network. In *Conference on Computer Vision and Pattern Recognition*, pages 6199–6208, 2018.

[24] Ming-Yu Liu and Oncel Tuzel. Coupled generative adversarial networks. In D. Lee, M. Sugiyama, U. Luxburg, I. Guyon, and R. Garnett, editors, *Advances in Neural Information Processing Systems*, volume 29. Curran Associates, Inc., 2016.

[25] Andrew Brock, Theodore Lim, James M. Ritchie, and Nick Weston. Neural photo editing with introspective adversarial networks. In *International Conference on Learning Representations*. OpenReview.net, 2017.

[26] Xudong Mao, Qing Li, Haoran Xie, Raymond YK Lau, Zhen Wang, and Stephen Paul Smolley. Least squares generative adversarial networks. In *International Conference on Computer Vision*, pages 2794–2802, 2017.

[27] Ian Goodfellow, Jean Pouget-Abadie, Mehdi Mirza, Bing Xu, David Warde-Farley, Sherjil Ozair, Aaron Courville, and Yoshua Bengio. Generative adversarial nets. *Advances in neural information processing systems*, pages 698–704, 2014.

[28] Tim Salimans, Ian Goodfellow, Wojciech Zaremba, Vicki Cheung, Alec Radford, and Xi Chen. Improved techniques for training gans. *Advances in neural information processing systems*, 29:2234–2242, 2016.

[29] Keith Ito and Linda Johnson. The lj speech dataset. <https://keithito.com/LJ-Speech-Dataset/>, 2017.

[30] Gyeong-Hoon Lee, Tae-Woo Kim, Hanbin Bae, Min-Ji Lee, Young-Ik Kim, and Hoon-Young Cho. N-Singer: A Non-Autoregressive Korean Singing Voice Synthesis System for Pronunciation Enhancement. In *Interspeech*, 2021.

- [31] Ilya Loshchilov and Frank Hutter. Decoupled weight decay regularization. In *International Conference on Learning Representations*, 2019.
- [32] Robert Kubichek. Mel-cepstral distance measure for objective speech quality assessment. In *Pacific Rim Conference on Communications Computers and Signal Processing*, volume 1, pages 125–128. IEEE, 1993.
- [33] Zhou Wang, Alan C Bovik, Hamid R Sheikh, and Eero P Simoncelli. Image quality assessment: from error visibility to structural similarity. *Transactions on Image Processing*, 13(4):600–612, 2004.
- [34] Antony W Rix, John G Beerends, Michael P Hollier, and Andries P Hekstra. Perceptual evaluation of speech quality (pesq)-a new method for speech quality assessment of telephone networks and codecs. In *International Conference on Acoustics, Speech and Signal Processing*, volume 2, pages 749–752. IEEE, 2001.
- [35] Cees H Taal, Richard C Hendriks, Richard Heusdens, and Jesper Jensen. A short-time objective intelligibility measure for time-frequency weighted noisy speech. In *International Conference on Acoustics, Speech and Signal Processing*, pages 4214–4217. IEEE, 2010.
- [36] Takuma Okamoto, Kentaro Tachibana, Tomoki Toda, Yoshinori Shiga, and Hisashi Kawai. Sub-band WaveNet with overlapped single-sideband filterbanks. In *Automatic Speech Recognition and Understanding Workshop*, pages 698–704. IEEE, 2017.

## A Detailed architecture

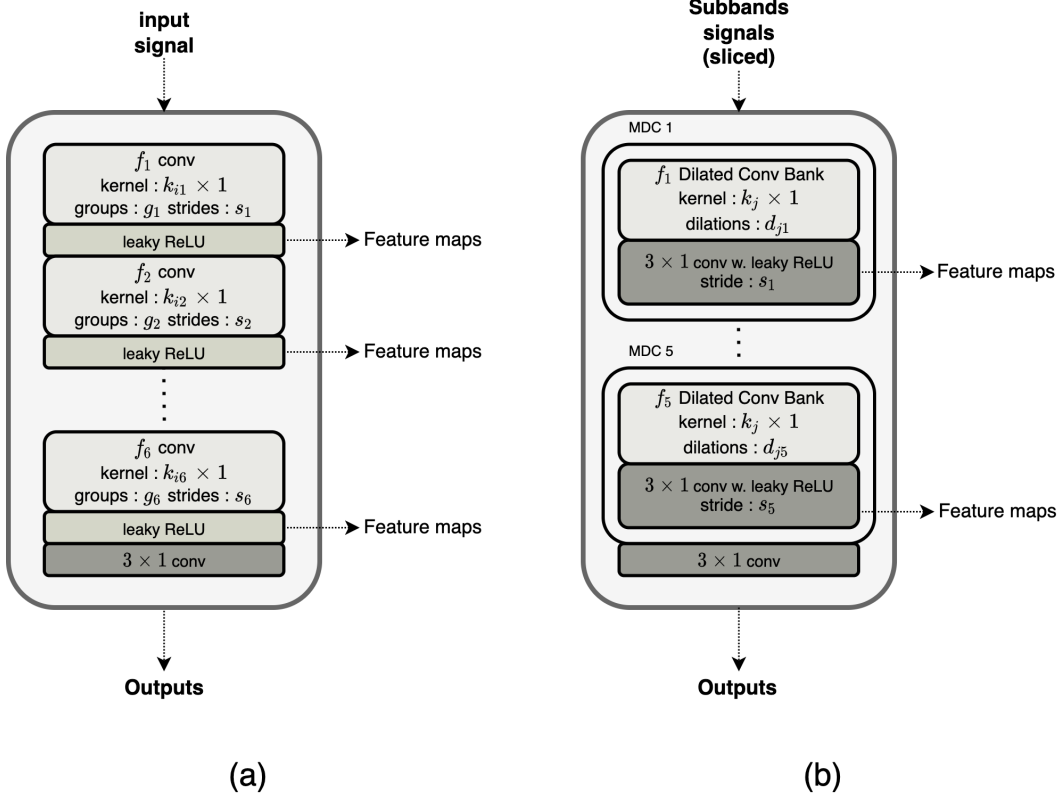


Figure 5: Detailed architectures of the sub-modules of the (a) Collaborative Multi-Band Discriminator and of the (b) Sub-Band Discriminator.

### A.1 Collaborative Multi-Band Discriminator

The architecture of the sub-module of the CoMBD is based on a discriminator block of the multi-scale discriminator (MSD) in MelGAN [11]. However, we set the hyper-parameters of the sub-modules of the CoMBD different from the MelGAN. The sub-modules are equipped with different receptive fields for each resolution unlike MSD. Detailed hyper-parameters of CoMBD are described in Table 6. Each sub-discriminator module is a Markovian window-based discriminator that can be established using strided convolutional layers [11]. Additionally, grouped convolution layers are also used to maintain the number of parameters while increasing the number of filters of the convolutional layer.

Table 6: The hyper-parameters of CoMBD.

	CoMBD <sub>1</sub>	CoMBD <sub>2</sub>	CoMBD <sub>3</sub>
Kernel size	[7, 11, 11, 11, 11, 5]	[11, 21, 21, 21, 21, 5]	[15, 41, 41, 41, 41, 5]
Kernel filters		[16, 64, 256, 1024, 1024, 1024]	
Kernel groups		[1, 4, 16, 64, 256, 1]	
Kernel stride		[1, 1, 4, 4, 4, 1]	

### A.2 Sub-Band Discriminator

The sub-modules of the SBD evaluate the sliced or the entire sub-band signals obtained by the PQMF analysis. Each sub-module comprises MDC layers in [25], as shown in Figure 5. The MDC

layer includes a convolution bank, a post-convolution layer, and a leaky ReLU activation layer. The convolution layers in the bank share kernel size but not dilation rates. Table 7 describes the hyper-parameters of SBD. The three sub-modules, i.e., tSBD, observe the changes in spectral features based on the time axis. We require each sub-module to cover a different range of frequency bands using different receptive fields. Consequently, the sub-module for low-frequency bands has large receptive fields, whereas the sub-module for broad frequency bands, it has small receptive fields.

Table 7: The hyper-parameters of SBD. The notation of sub-band range  $[x:y]$  means that  $x$ th to  $y$ th sub-band signals are selected.

	tSBD <sub>1</sub>	tSBD <sub>2</sub>	tSBD <sub>3</sub>	fSBD
Kernel size	7	5	3	5
Kernel filters		[64, 128, 256, 256, 256]		[32, 64, 128, 128, 128]
Kernel stride	[1, 1, 3, 3, 1]	[1, 1, 3, 3, 1]	[1, 1, 3, 3, 1]	[1, 1, 3, 3, 1]
Dilation factor	[5, 7, 11]×5	[3, 5, 7]×5	[1, 2, 3]×5	[1, 2, 3]×3, [2, 3, 5]×2
Sub-band range	[1:6]	[1:11]	[1:16]	[1:64]

## B Pseudo Quadrature Mirror Filter bank

Various types of digital filter banks are commonly used to inspect the frequency information of speech or image signals. Perfect decomposition and reconstruction are the key features of a digital filter. The quadrature mirror filter (QMF) bank is one of the most prevalent filters that can perfectly decompose and reconstruct a target signal. [20] proposed a pseudo-QMF (PQMF) bank based on the cosine modulated filter. The PQMF comprises an analysis and synthesis filter for multi-band sub-coding. In particular, PQMF has stopband attenuation over 100dB, appropriate for sub-band coding without aliasing. Since it is possible to decimate speech signals without distortion, several neural vocoders employ the PQMF to achieve computational efficiency [14, 21, 36]. Table 8 describes the hyper-parameters of PQMF based on the number of sub-bands. These values were selected empirically to prevent artifacts during decimation.

Table 8: The hyper-parameters of PQMF.

	Number of sub-bands			
	2	4	16	64
Taps	256	192	256	256
Cut-off ratio	0.25	0.13	0.03	0.1
Beta	10.0	10.0	10.0	9.0

## C Analysis on singing voice synthesis

We observed that the HiFi-GAN could not reconstruct waveforms comprising which fundamental frequencies are higher than 750Hz, as shown in Figure 6. We highly recommend hearing these audio samples at an our sample page in Appendix D. Downsampling using an equally spaced sampling, as in MPD, can be the reason for incompleteness. When the waveform is downsampled with the equally spaced sampling over a large period, such as 11, the components of second harmonic fold down and are located at a lower position than the first harmonic components due to the aliasing.

The high-frequency components are sparsely present in the training data. The existence of aliasing is fatal for the discriminator to discriminate these sparse data. Consequently, the aliasing prevents the generator from learning to reconstruct the high-frequency components accurately. This result is similar to the difference in generalization between Avocodo and HiFi-GAN, as confirmed by the unseen speaker synthesis experiment in Section 5.1.

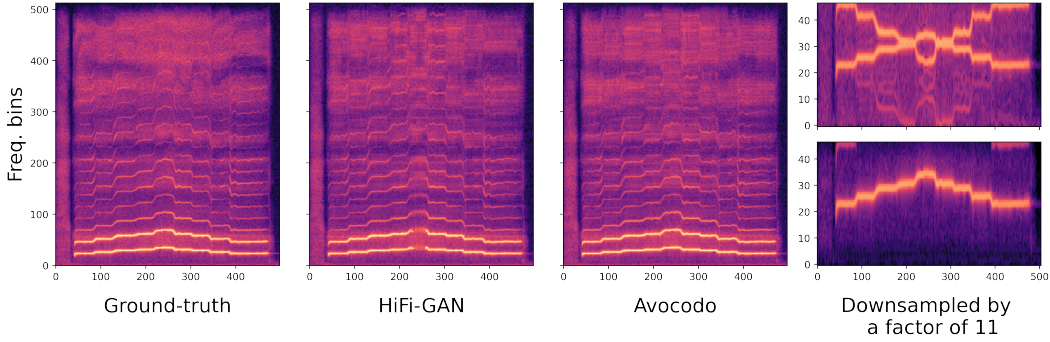


Figure 6: The first three spectrograms are from a ground-truth vocal scales audio, synthesized audio by HiFi-GAN V1 and Avocodo V1, respectively. Two spectrograms on the last column shows the spectrograms of downsampled audio by a factor of 11: **Up**: Downsampling using the equally spaced sampling causes the aliasing. **Down**: Downsampling using PQMF analysis.

## D Sample page

All audio samples are available at <https://nc-ai.github.io/speech/publications/Avocodo/index.html>.